Effect of Strain Rate on the Yield Stress of Ferritic Stainless Steels

KESTER D. CLARKE, ROBERT J. COMSTOCK, Jr., MARTIN C. MATAYA, CHESTER J. VAN TYNE, and DAVID K. MATLOCK

The effect of strain rate on the yield stress of ferritic stainless steel sheet was experimentally determined and a previously developed model was applied to the data. Five ferritic stainless steel alloys, including one in two thicknesses, were mechanically tested at room temperature in uniaxial tension at strain rates ranging from 0.001 to 300 s^{-1}, and low-strain-rate tests were selectively performed at nonambient temperatures. The hypothesis that ferritic stainless steels react similarly to strain rate as mild steels was investigated by the application of a widely accepted strengthening model, based on body-centered-cubic (bcc) crystal lattice deformation mechanisms, to the experimental data.[1] Yield stresses were compared to model predictions and good agreement was found. The results allow for the prediction of yield stresses for these materials over strain rate ranges of 0.001 to 300 s^{-1}, and as a function of test temperature. Model parameters for the ferritic stainless steels were reasonable relative to those previously reported for pure bcc ferritic iron.[1] A correlation between the effect of alloying additions on solid solution strengthening and the athermal component of shear stress is also suggested. The results allow prediction of yield stress of ferritic stainless steels over a wide range of strain rates and temperatures.

DOI: 10.1007/s11661-008-9479-4

I. INTRODUCTION AND BACKGROUND

THE excellent corrosion resistance and reasonable cost of ferritic stainless steel alloys make this class of materials important to the forming industry. Specific application of these materials includes automotive exhaust components, from the exhaust manifold to the tailpipe. Common stamped parts include catalytic converter housings, heat shields, stamped mufflers, and hydroformed exhaust tubing. Generally, AISI 409 (Cr ~10 wt pct) is primarily used for exhaust applications, while AISI 439 and 18 Cr-Cb (Cr ~18 wt pct) are generally used on some demanding "hot" end applications (exhaust manifold to catalytic converter), where improved oxidation resistance is desired. These exhaust applications are becoming more challenging from a forming standpoint, as limited space in the undercarriage of modern vehicles requires exhaust components to be routed in indirect and complex ways. The lack of published mechanical property data with respect to strain rate and temperature in these higher alloy materials results in increased challenges during process development and production.

Under certain conditions, the ductile-to-brittle transition temperature in ferritic stainless steels is at temperatures as high or higher than ambient.[2,3] In addition, the yield stress varies significantly with temperature and strain rate, which also affects formability. Thus, it has been recommended that ferritic stainless steels should not be formed in conditions under 10 °C (283 K), especially in higher Cr compositions or thicker sheets.[3] If ambient or outside (if material is delivered on a just-in-time basis) temperatures are less than 16 °C (289 K), the material should be allowed to warm (temperature effect) prior to forming and the forming speed should be decreased (strain rate effect) to prevent cracking and achieve the desired formability.[3] In addition, it is recommended that thinner and lower alloyed material be formed first, allowing the tooling and thicker high alloy material to warm, thereby increasing the probability of forming good parts with the thicker or higher alloyed materials.[3]

Developing correlations between mechanical properties, processing conditions, and the final performance of the material will allow the advantages of ferritic stainless steels to be exploited in more difficult forming applications. In this regard, the ability to predict the yield stress of these ferritic stainless steels is critical when determining input parameters for finite element models to predict forming characteristics. This article reports results from high-strain-rate tensile testing and the application of a screw dislocation kink-pair interaction model previously

KESTER D. CLARKE, Graduate Research Assistant, MARTIN C. MATAYA, Physical Metallurgy Lecturer, CHESTER J. VAN TYNE, FIERF Professor, and DAVID K. MATLOCK, Charles F. Fogarty Professor, are with Advanced Steel Processing and Products Research Center, Colorado School of Mines, Golden, CO 80401. Contact e-mail: kclarke@mines.edu ROBERT J. COMSTOCK, Jr.,Senior Research Engineer, is with the Research and Technical Services Division, AK Steel Corporation, Middletown, OH 45043.

This article is based on a presentation made in the symposium entitled "Dynamic Behavior of Materials," which occurred during the TMS Annual Meeting and Exhibition, February 25–March 1, 2007 in Orlando, Florida, under the auspices of The Minerals, Metals and Materials Society, TMS Structural Materials Division, and TMS/ASM Mechanical Behavior of Materials Committee.

Article published onlined February 22, 2008

developed by Seeger and Schiller[4] and applied by Brunner and Diehl[1,5–10] to predict yield stresses over a range of strain rates and temperatures. The outcome of experimental testing and modeling results is the ability to predict yield stresses for five ferritic stainless steels over strain rate ranges of 0.001 to 300 s^{-1}, and as a function of test temperature.

A summary of the deformation behavior of iron follows as a basis for the theory behind the expected deformation behavior of the ferritic stainless steels tested here, and the model that is used to fit the experimental data.

A. *Deformation Behavior of Iron Single Crystals*

In body-centered-cubic (bcc) iron single crystals, it has been established and summarized by Spitzig and Keh[11] that the predominant active slip planes are the {110}- and {112}-type planes over temperatures ranging from 143 to 573 K. The active slip system is dependent on temperature and imposed strain rate.

Brunner and Diehl[1,5–10] performed a series of stress relaxation experiments relating the tensile flow stress of high-purity ferritic-iron single crystals to temperature and strain rate. Single crystals were studied at different orientations and the resolved shear stress was calculated by the Schmid factor for (011)[111] slip. Crystals were deformed in tension at a shear strain rate of 8.5×10^{-4} s^{-1} and at different temperatures. At each temperature the crystal was deformed at increments of up to 2 pct strain, and toward the end of each deformation the cross head was stopped. The load then decreases with time because of plastic deformation continuing in the sample due to thermally active screw dislocations. For a sufficiently stiff machine, the stress relaxation test can provide the yield stress dependence on temperature and strain rate. For temperatures above 250 K and strain rates below 1000 s^{-1}, the primary mechanism of slip in bcc materials is screw dislocation motion, controlled by nucleation[6] and migration of kink pairs.[9]

B. *Deformation Behavior of Iron Polycrystals*

In pure ferritic-iron polycrystals, the effects of strain rate can be considered qualitatively by considering how the mechanical properties change with temperature. Figure 1 shows the temperature dependence of the 0.2 pct offset tensile yield stress with respect to temperature in pure ferritic iron that was gettered with titanium to remove interstitial solute atoms.[12] The strain rate (2.5×10^{-4} s^{-1}) and grain size (ASTM 5 to 6, approximately 44 to 63 μm) were held constant for all of the tests. Although Figure 1 plots 0.2 pct offset yield stress as a function of temperature at a constant strain rate, the effects of strain rate on yield stress are considered to be analogous to these temperature effects; *i.e.*, it is assumed that a similar plot could be obtained by varying strain rate and holding temperature constant, because an increase in strain rate is analogous to a decrease in temperature.

There are four distinct temperature regimes as shown in Figure 1.

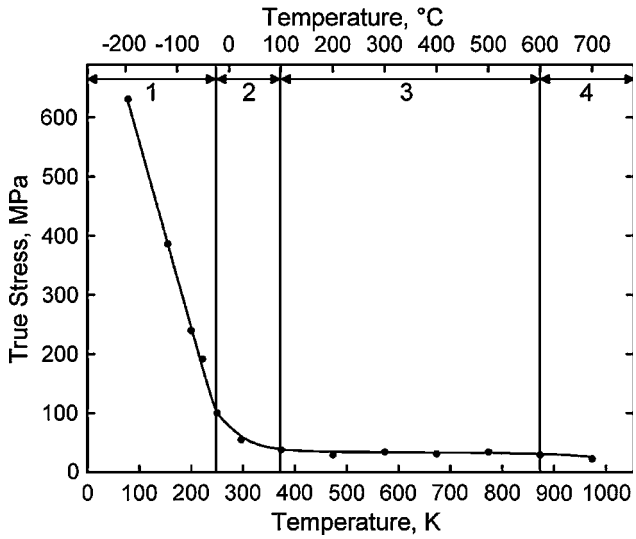

Fig. 1—Temperature dependence of the 0.2 pct offset lower tensile yield stress of pure ferritic iron (ASTM grain size 5 to 6, approximately 44 to 63 μm) at a strain rate of 2.5×10^{-4} s^{-1} (adapted from Ref. 12, regime separations were added to the original plot).

(1) A linear portion below room temperature (300 K) extending from 80 to 250 K, where the yield stress is strongly dependent on temperature (and strain rate).
(2) A transition regime around room temperature from 250 to 373 K, where the dependence of the yield stress on temperature (and strain rate) decreases rapidly as temperature increases.
(3) A linear portion well above room temperature extending from 373 to 873 K, where the yield stress is mildly dependent on temperature (and strain rate), declining in proportion to the decrease in elastic modulus with increasing temperature.
(4) A region above 873 K, where the yield stress declines more rapidly with increasing temperature (or decreasing strain rate).

In Figure 1, regimes 1, 2, and 4 are considered to be thermally activated. In other words, the shear stress required for plastic deformation is dependent on the temperature and strain rate at which the material is deformed. Specifically, in regimes 1 and 2, the strain rate and temperature dependence of the yield stress are attributed to the difficulty in moving screw dislocations at low temperatures (or high strain rates) due to periodic energy barriers (Peierl's stress), interstitial impurities, or thermally-activated sessile-glissile conversions of screw dislocations.[12] Because increasing strain rate is analogous to decreasing the temperature in thermally-activated processes, a significant strain rate sensitivity is expected in pure ferritic iron in room-temperature tensile tests. When deformation occurs at quasi-static strain rates (*e.g.*, 2.5×10^{-4} s^{-1} in Figure 1), 250 K is accepted as the transition temperature between the strongly temperature dependent and weakly temperature dependent regimes.[6–8] Regime 3, however, displays behavior that is considered athermal, where the shear stress required for yielding is dependent only on the state of the material (dislocation density), lattice

structure, and shear modulus. The flow stress in regime 4 decreases linearly as a function of increasing temperature, and the slope of the true stress *vs* temperature curves in this region become more negative with increasing strain. In addition, the temperatures that define the boundaries of the four regimes are also likely to be strain rate dependent. Therefore, it follows that the controlling deformation mechanism in ferritic iron would respond similarly to an increase in strain rate or a decrease in temperature.

It follows that the total shear stress, τ_{total}, required for deformation can be considered as the sum of the athermal and thermal components

$$\tau_{\text{total}} = \tau_G + \tau^*(T, \dot{\varepsilon}) \quad [1]$$

$$\tau_G = \alpha' \cdot G \cdot \mathbf{b} \cdot \rho^{1/2} \quad [2]$$

where τ_G represents the athermal component of the shear stress, τ^* represents the thermal component of the shear stress and is dependent on temperature T, and strain rate $\dot{\varepsilon}$, G is the shear modulus of the material, $\mathbf{b}$ is the lattice burger's vector, ρ is the total dislocation density, and α' is a material-specific proportionality constant.[13]

C. *Low-Carbon Steel*

Figure 2 correlates the yield stress of low-carbon steel with changes in strain rate and temperature;[14] the observed behavior is analogous to the effect of temperature on the flow stress of pure iron (Figure 1), where an increase in strain rate is assumed equivalent to a decrease in temperature. For the purposes of this study, regions I and II are important.

In Figure 2, region I shows little effect of temperature or strain rate on flow stress (analogous to regime 3 in Figure 1). Region II shows that strain rate and temperature have a measurable effect (analogous to regime 2 in Figure 1), and that the yield stress increases with strain rate up to a strain rate of 5000 s^{-1}.

Controlling mechanisms are generally accepted and are summarized as follows for regions I and II in Figure 2.[14]

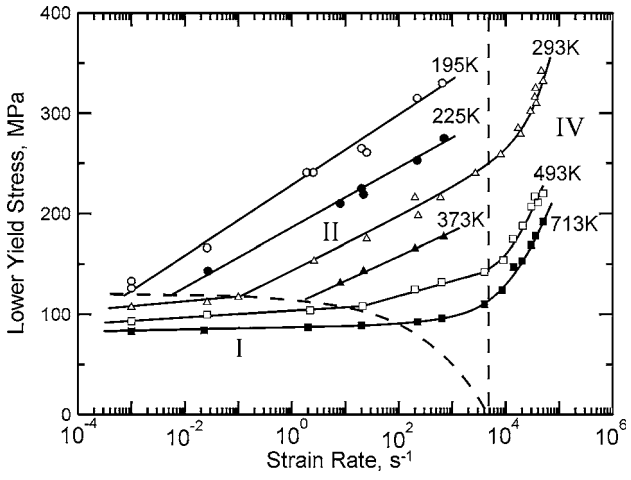

Fig. 2—Strain rate and temperature dependence of the lower yield stress for an annealed mild steel (adapted from Ref. 14).

(I) Low strain rates and high temperatures, where flow is controlled by long-range friction stresses that are not able to be overcome by thermal vibration assistance. The athermal stress, τ_G, increases with alloy content.

(II) Higher strain rates and low temperatures, where flow is controlled by short-range barriers to flow such as dislocation interactions. Thermal vibrations are able to assist in overcoming these barriers, and flow becomes sensitive to strain rate and temperature. This behavior can be described by an Arrhenius-type relationship, which is a function of the thermal component of shear stress, temperature, and a nominal strain rate.

These basic strain rate and temperature effects are characteristic of low-carbon steels. In region I, the increase in the athermal component of stress without a disruption in the thermal component of stress tends to reduce the visible effect of strain rate and temperature on the materials that are considered here (*i.e.*, the athermal component becomes a larger percentage of the total stress).[14] Therefore, at room temperature a significant strain rate and temperature dependence of the yield stress is expected in low-carbon steels.

II. MODEL THEORY

Based on the correlation between temperature and strain-rate effects in bcc polycrystals, a theory of plastic behavior in pure bcc metals has been proposed by Seeger and Schiller.[4,15] A key component of this model is the assumption that the critical resolved shear stress τ is described by Eq. [1].

It has been reported that plastic flow in bcc metals at temperatures between 250 and 500 K is limited by the formation of kink pairs in screw dislocations.[6] The strain rate $\dot{\varepsilon}$ has been shown to be a function of the burger's vector $\mathbf{b}$, screw dislocation density N_d, and the average dislocation velocity v_d:[16]

$$\dot{\varepsilon} = \mathbf{b} \cdot N_d \cdot v_d \quad [3]$$

The average dislocation velocity is a function of the length a kink can travel before reaching an insurmountable barrier L, the kink height a, and the net rate of formation of kink pairs Γ_k. The strain rate can now be written as follows:[16]

$$\dot{\varepsilon} = \mathbf{b} \cdot N_d \cdot L \cdot a \cdot \Gamma_k \quad [4]$$

The form of Γ_k has been given by Seeger:[16]

$$\Gamma_k = C \cdot \exp[-H_{kp}(\tau^*)/k \cdot T] \quad [5]$$

$$C = (\pi \cdot m_k \cdot \mathrm{k} \cdot T)^{-1/2} \left(2\pi \cdot H_k / w_k^2\right) \quad [6]$$

where $H_{kp}(\tau^*)$ is the enthalpy of formation of a kink-pair, k is Boltzmann's constant, m_k is the mass of a kink, w_k is the width of the kink, and T is the absolute temperature. For the purposes of this study, it was assumed that C can be approximated as a constant.[16]

Equations [3] through [5] can be combined to yield the following expressions:[16]

$$\dot{\varepsilon} = \mathbf{b}\cdot N_d\cdot L\cdot a\cdot C\cdot \exp[-H_{kp}(\tau^*)/k\cdot T] \quad [7]$$

$$\dot{\varepsilon} = \dot{\varepsilon}_o\cdot \exp[-H_{kp}(\tau^*)/k\cdot T] \quad [8]$$

where $\dot{\varepsilon}_o$ can be approximated as a constant[16] that contains the burger's vector **b**, the screw dislocation density N_d, the length a kink can travel before reaching an insurmountable barrier L, the kink height a, and the approximated constant C of Eqs. [5] and [6].

In order for a kink pair to be developed, a portion of the screw dislocation must overcome the Peierl's barrier. Stress can provide assistance to the thermal fluctuations in energy of a dislocation, allowing it to more easily overcome this barrier. Therefore, the kink-pair formation enthalpy is a function of stress, as illustrated in Eqs. [5] and [7]. If there is sufficient separation between kinks, such that the energy barrier is well defined, the kink-kink interaction enthalpy can be calculated using a Coulomb-type interaction.[15] The kink-pair formation enthalpy can then be calculated as follows:[15,16]

$$H_{kp}(\tau^*) = 2H_k - H_{kk}(\tau^*) \quad [9]$$

$$H_{kp}(\tau^*) = 2H_k - 2\alpha(\tau^*)^{1/2} \quad [10]$$

where H_k is the enthalpy of an isolated kink, $H_{kk}(\tau^*)$ is the kink-kink interaction enthalpy, and α is a material specific parameter that is dependent on alloying content and dislocation density.[6]

Equations [1], [8], and [10] define the relationship between temperature and strain rate for bcc metals in terms of the enthalpy of an isolated kink H_k, and two constants, $\dot{\varepsilon}_o$ and α, at temperatures where the formation rate of kink pairs limits plastic deformation. Combining Eqs. [1], [8], and [10], the following relationship can be reached:

$$\tau_{\text{total}} = \tau_G + [(\ln(\dot{\varepsilon}/\dot{\varepsilon}_o)\mathrm{k}\cdot T + 2H_k)/2\alpha]^2 \quad [11]$$

In Eq. [11], the parameters $\dot{\varepsilon}$, k, and T are known, and the parameters τ_G, $\dot{\varepsilon}_o$, H_k, and α are unknown. This allows these parameters to be varied to fit strain-rate-dependent yield stresses determined experimentally within the temperature regime applicable to the model.

Brunner and Diehl[1,5–10] applied the model to tensile stress relaxation measurements in high-purity ferritic iron. As stated earlier, it was reported by Brunner and Diehl[8] that 250 K is an approximate transition temperature for a change in the primary screw dislocation motion from the {110} slip planes to the {112} slip planes, which are the active slip planes up to 500 K. Below 250 K, it was found that the value of $\dot{\varepsilon}_o$ changes slightly, resulting in a discontinuity in the predicted yield stress *vs* temperature curve.[8]

The application of this model to a polycrystalline ferritic stainless steel has not previously been attempted, and the experimental data compiled for this study provides the opportunity to evaluate the applicability of the previously developed model based on the theory of plastic deformation behavior in bcc metals[4,15–17] to ferritic stainless steels. This model has previously been applied to pure ferritic iron[1,5–10] and niobium,[16] but not to ferritic stainless steels. The significance of this study is to couple a limited-use theory for pure materials to the deformation mechanisms present in real engineering materials, specifically ferritic stainless steels. The major assumption of the model is that the strain rate sensitivity of the ferritic stainless steels is controlled by deformation in the ferrite phase. The difference in ferrite phase deformation stress between the pure materials and the ferritic stainless steels is alloying, and the corresponding effect of alloying on short- and long-range obstacles to dislocation motion.

III. MATERIALS AND EXPERIMENTAL PROCEDURE

A. *Material*

The five commercial sheet materials used in this study were HIGH PERFORMANCE-10* 409 (HP-409), ULTRA FORM** 409 (UF-409), 18 Cr-Cb,* HIGH PERFORMANCE-10* 439 (HP-439), and Duracorr.†

*HP-409, 18 Cr-Cb, and HP-439 are the trademarks of AK Steel, Middletown, OH.

**UF-409 is a registered trademark of AK Steel, Middletown, OH.

†Duracorr is a registered trademark of Bethlehem Steel Company, now ArcelorMittal, Bethlehem, PA.

The chemical composition, grain size, and thickness of each material are presented in Table I. Two thicknesses of the 18 Cr-Cb alloy were used. All alloys have a ferritic matrix and were supplied in the annealed condition. Table I also shows the grain size term $d^{-1/2}$ from the Hall–Petch relation.[18]

$$\sigma_y = \sigma_o + k_y d^{-1/2} \quad [12]$$

where σ_y is the yield stress, d is the grain size, and σ_o and k_y are the usual Hall–Petch parameters. The grain size effect (proportional to $d^{-1/2}$) for HP-409, UF-409, HP-439, and 18 Cr-Cb (1.6 mm) are essentially the same. The grain size of 18 Cr-Cb (1.2 mm) is slightly larger, although this has a relatively small effect on Hall–Petch strengthening. Duracorr has a much smaller grain size that significantly increases the Hall–Petch strengthening effect.

However, the two thicknesses of 18 Cr-Cb are not from the same heat of steel.

B. *Tensile Testing*

Uniaxial tensile tests were performed on the five ferritic stainless steels in Table I at strain rates ranging from 0.001 to 300 s^{-1}. Yield stress was determined using the 0.2 pct offset yield stress for each of the materials. Further details regarding methods have been published elsewhere,[19–22] and an overview follows.

A high-strain-rate testing method was developed[19–22] and tensile tests were performed using a commercial high-rate servohydraulic testing machine. The high-rate testing system was capable of actuator velocities up to 10 m/s under load, and the actuator was equipped with a slack-adapter fixture to allow actuator acceleration to the desired velocity prior to engaging the sample. Tensile testing was performed on all five materials (including the two different thicknesses of 18 Cr-Cb) at strain rates between 0.001 and 300 s^{-1}. Tensile samples were machined with the tensile axis parallel to the rolling direction. For tests of 100 s^{-1} and below, a gage length of 50 mm (2 in.) and a gage width of 13 mm (0.5 in.) was used. At the highest rates (>100 s^{-1}), a subsized specimen with a gage section of 25 mm (1 in.) and a gage width of 6 mm (0.25 in.) was used. Strain was measured with high-elongation strain gages (up to 0.15 strain) attached directly to the reduced gage section on each sample.[19,20] Low strain rate studies showed excellent agreement between strain data measured with high elongation strain gages and conventional extensometers.[19–23]

At low rates, a standard piezoelectric load washer provided accurate and reliable load data. However, for rates of 10 s^{-1} and above, noise and ringing (*i.e.*, fluctuations in the load signal) were prevalent in the load signal, as would be expected due to the sudden sample engagement by the slack adapter. The effect of "ringing" on the load signal was minimized by using low mass grips and measuring load directly with an elastic strain gage mounted to one grip section of each sample.[19,20] The grip section strain gage signal was calibrated to the load washer signal in tests performed at low rates, and then used to determine loads during testing at high strain rates. The grip strain gage method was found to be reliable up to the point where the strain in the gage section reached 0.05 to 0.15, at which point the elastic grip gage began to debond from the grip section.

The gradual debonding of the grip-gage necessitated the development of a procedure to analyze load data above gage strain values of approximately 0.05. For gage strains above 0.05, load washer data were processed through a curve smoothing routine, in order to determine average load *vs* time profiles. The smoothed values were used for the loads at strains above which the grip strain gage debonded.[19,20]

The yield stress for each set of data was determined using the 0.2 pct offset yield stress. The mean 0.2 pct offset yield stress of a minimum of five tensile tests was averaged to reach the final yield stress. At a strain rate of 0.1 s^{-1}, the yield stress repeatability was determined to be ± 5 MPa when comparing the strain-gage method with traditional tensile tests employing a standard extensometer. This accuracy is considered to be consistent from the lowest rates tested up to a strain rate of 1 s^{-1}. At strain rates of 10 s^{-1} and above, the data near the yield point exhibited increased variability. The 0.2 pct offset yield stress showed variation in repeated tests of up to ± 30 MPa in the worst case, and averaged ± 20 MPa. The final curves were an average of a set of at least three tests. A record of each set of tests is available in Reference 19, and Figure 3 presents a representative set of truncated true stress *vs* true strain curves for the 18 Cr-Cb (1.6 mm) material.

Table I. Chemical Composition (Weight Percent), ASTM Grain Size, and Thickness of the Five Experimental Ferritic Stainless Steel Alloys

Alloy	HP-409	UF-409	HP-439	18 Cr-Cb	18 Cr-Cb*	Duracorr
Thickness, mm	1.4	1.4	1.4	1.2	1.6	1.7
ASTM grain size	7.8	8.4	7.9	6.6	8.6	11.0
Grain size, μm	24.0	19.5	23.2	36.5	18.2	7.9
Hall–Petch term, $d^{-1/2}$ $mm^{-1/2}$	6.4	7.2	6.6	5.2	7.4	11.3
Cr	10.83	11.18	17.31	18.25	—	11.37
Ni	0.15	0.14	0.19	0.31	—	0.41
C	0.008	0.009	0.007	0.014	—	0.017
Mn	0.17	0.18	0.20	0.29	—	1.43
Si	0.38	0.34	0.36	0.40	—	0.66
Nb	0.004	0.004	0.007	0.54	—	0.002
Ti	0.20	0.18	0.30	0.21	—	0.001
Al	0.016	0.008	0.025	0.020	—	0.008
Cu	0.09	0.11	0.08	0.09	—	0.07
Mo	0.03	0.03	0.04	0.04	—	0.25
Co	0.02	0.02	0.02	0.02	—	—
V	0.068	0.063	0.102	0.090	—	0.027
P	0.019	0.021	0.023	0.02	—	0.021
Sn	0.008	0.009	0.010	0.015	—	—
S	0.001	0.001	0.001	—	—	0.003
N	0.011	0.007	0.010	0.014	—	0.0114

*The composition of the 18 Cr-Cb (1.6 mm) material is not shown here, although it is nominally the same as the 18 Cr-Cb (1.2 mm).

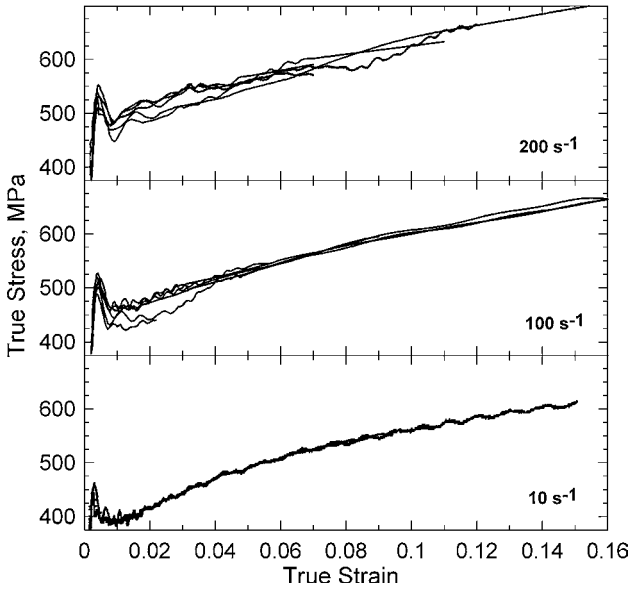

Fig. 3—Sets of true stress *vs* true strain curves for the 1.6-mm-thick 18 Cr-Cb material at strain rates of 10, 100, and 200 s^{-1}. These sets of tests give an indication of the variability and repeatability of a high-rate tensile test.

In addition to varying strain rate at room temperature, tensile tests were performed at 250 K for two relatively low strain rates (approximately 0.0001 and 0.001 s^{-1}) for each material. These tests were performed using an electromechanical tensile testing machine with the sample immersed in a 250 K ethanol bath.

Elevated temperature tensile tests were performed at a strain rate of 0.0001 s^{-1}, using the 1.2-mm-thick 18 Cr-Cb material. Tests were performed on a servohydraulic tensile testing machine with an in-line resistance furnace. Temperatures were monitored throughout the test using thermocouples attached to the gage section of the samples.

IV. RESULTS

After determining yield strengths for each of the materials, two methods for fitting the model function (Eq. [11]) to the experimental data were considered: (1) an automatic least-squares nonlinear regression and (2) a controlled manual fit determined by forcing a fit through 300 K and 0.01 s^{-1} experimental data points, followed by manual manipulation of the model parameters. The saturation strain rate $\dot{\varepsilon}_o$ was considered to be constant for each of the five alloys, since the dislocation density was assumed to be similar for the continuously annealed experimental materials. The kink enthalpy H_k is dependent on alloying content, and the parameter α is dependent on material condition (dislocation density) in addition to alloying content. Therefore, H_k and α were both allowed to vary for each of the alloys. The athermal component of the flow stress τ_G is simply based on the flow stress of the base bcc matrix, plus typical long-range solid solution strengthening effects. Considering a pure iron ferrite matrix, τ_G is dependent on solid solution alloy additions, dislocation structure, and grain size.

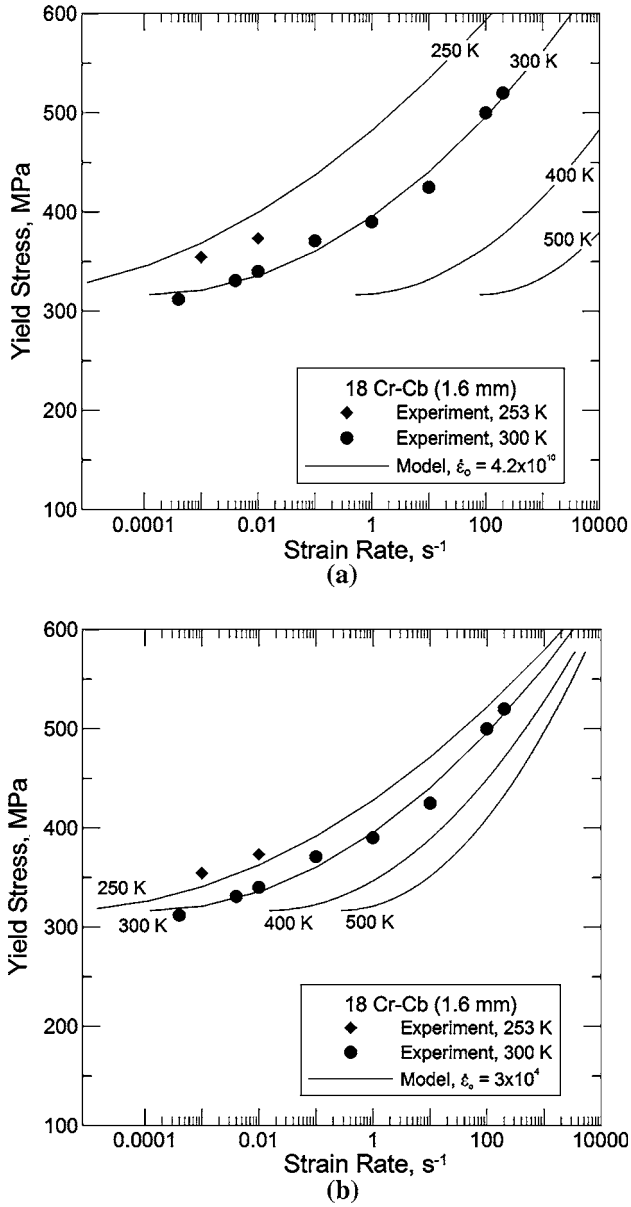

Fig. 4—Experimental 0.2 pct offset yield stress data plotted with nonlinear least-squares regression model predictions as a function of strain rate and temperature for 18 Cr-Cb (1.6 mm).

The nonlinear least-squares regressions were performed using a constant value for $\dot{\varepsilon}_o$ and using τ_G, H_k, and α as dependent parameters to fit the room-temperature experimental data. A value of $\dot{\varepsilon}_o = 4.2 \times 10^{10}\ s^{-1}$ was used based on the reported value presented in the literature for pure ferritic iron.[1] Figure 4(a) shows the resulting nonlinear least-squares regression results (lines) plotted with experimental data (symbols). For this fit, the values for the dependent parameters are as follows: $\tau_G = 158$ MPa, $H_k = 0.87$ eV, and $\alpha = 1.86 \times 10^{-5}$ m eV/$N^{1/2}$. Values for the dependent parameters are reasonable relative to the reported values in literature,[1] with exception of a high value of τ_G. The model fit for the

Table II. Model Parameters from Literature and for the Five Experimental Ferritic Stainless Steel Alloys

Material	$2H_k$ (eV)	α (m eV/N$^{1/2}$)	$\dot{\varepsilon}_o$ (s^{-1})	τ_G (MPa)
Ferritic iron, from Ref. 1	0.92	1.94×10^{-5}	4.2×10^{10}	1
Nb, from Ref. 16	0.65	1.62×10^{-5}	1.4×10^{7}	33
HP-409	0.90	2.80×10^{-5}	3.0×10^{4}	33
UF-409	0.90	2.80×10^{-5}	3.0×10^{4}	39
HP-439	0.92	3.23×10^{-5}	3.0×10^{4}	78
18 Cr-Cb (1.6 mm)	0.95	3.23×10^{-5}	3.0×10^{4}	93
18 Cr-Cb (1.2 mm)	0.95	3.23×10^{-5}	3.0×10^{4}	98
Duracorr	1.00	3.85×10^{-5}	3.0×10^{4}	119

experimental yield stresses determined at room temperature is excellent. The high value for τ_G precludes a yield stress prediction below 316 MPa, regardless of test temperature, which is reinforced by the above room-temperature model predictions shown in Figure 4(a). In addition, the fit predicts a higher value than shown for the experimental low temperature tensile tests.

As a result, manual estimations of $\dot{\varepsilon}_o$ were performed to improve the fit with experimental data. A value of $\dot{\varepsilon}_o = 3.0 \times 10^4\ \text{s}^{-1}$ was found to give a more reasonable relative stress difference between tests performed at low temperature and room temperature. The change in $\dot{\varepsilon}_o$ may seem to be extremely large, but it is helpful to acknowledge that the logarithm of the $\dot{\varepsilon}_o$ is used in Eq. [11], and the difference between the logarithms of the two $\dot{\varepsilon}_o$ values is much less than an order of magnitude, given that the logarithm of $\dot{\varepsilon}_o$ changes only from 24.5 (ln 4.2×10^{10}) to 10.3 (ln 3.0×10^4). In addition, since $\dot{\varepsilon}_o$ is dependent on the dislocation density,[6,16] it is likely that the dislocation density of the experimental materials in this study have a significantly different dislocation density than the pure ferritic iron.

Figure 4(b) presents the results of the nonlinear least-squares regression using $\dot{\varepsilon}_o = 3.0 \times 10^4\ \text{s}^{-1}$. An excellent fit for the experimental yield stresses determined at room temperature is shown. Values for the dependent parameters are as follows: $\tau_G = 158$ MPa, $H_k = 0.50$ eV, and $\alpha = 1.86 \times 10^{-5}$ m eV/N$^{1/2}$. As in the fit using $\dot{\varepsilon}_o = 4.2 \times 10^{10}\ \text{s}^{-1}$, the value for τ_G is high, especially when considering that a value of 158 MPa for τ_G results in a minimum yield stress of 316 MPa, regardless of test temperature, which is reinforced by the room-temperature model predictions shown in Figure 4(b). The lower saturation of the predicted yield stress is a persistent and unavoidable problem for the nonlinear least-squares regression method for fitting the 300 K yield stress data determined in this study.

A controlled manual method for fitting the room-temperature experimental data was found to provide more reasonable results than the nonlinear least-squares regression method. The manual method of fitting Eq. [11] to the room-temperature experimental yield stresses used the parameters H_k, α, $\dot{\varepsilon}_o$, and τ_G to provide a best fit to the experimental data. The parameters were determined using plots of yield stress *vs* strain rate similar to Figures 4(a) and (b). The best fit of the experimental data was determined by forcing a fit through the 0.01 s^{-1} yield stress obtained at 300 K, using primarily the value for τ_G, because the athermal shear stress has the greatest effect on the magnitude of the total shear stress. In order to best match the slope and spacing of the curves, the parameters H_k and α were used to adjust the curves, as these parameters have the greatest effect the shape and relative spacing of the curves.

Table II presents the final model parameters used to predict yield stress for the experimental ferritic stainless steel alloys, as well as those used in previous work on pure ferritic iron[1] and niobium[16] for comparison.

Figure 5 presents yield stress *vs* strain rate results obtained from experiments (symbols) and predicted by the model (lines) for each of the five materials, including two thicknesses of 18 Cr-Cb. For each of the materials, the yield stress increases as a function of strain rate at a given temperature. In addition, it appears that the strain rate sensitivity of the materials increases at strain rates greater than 100 s^{-1}. The model predictions for temperatures other than room temperature have not generally been experimentally verified. However, the agreement between the model predictions and the small number of nonambient temperature tests that were performed indicate that these predictions may well be a reasonable to estimate yield stresses. In Figure 5, the 18 Cr-Cb (1.6 and 1.2 mm) data points plotted at 3000 s^{-1} were determined from a Split–Hopkinson Bar compression test,[19] were not included in the data during any of the fitting procedures, and are shown here for reference purposes only.

V. DISCUSSION

A. *Tensile Testing*

Experimental yield stress data, presented in Figure 5, exhibit similar trends to those shown for pure ferritic iron and low-carbon steels, presented in Figures 1 and 2, respectively. As expected, the yield stress increases as a function of strain rate in all cases, and each material displays a similar response to increasing strain rate, irrespective of the absolute value of the yield stress.

Based on the room-temperature experimental yield stress results, it appears that the strain rate sensitivity increases continuously with strain rate. A continuous strain-rate-sensitivity curve would suggest a single deformation mechanism over the strain rates tested.

B. *Yield Stress Model Fit*

The yield stress model employed here assumes that a single deformation mechanism applies to the strain rate (0.001 to 300 s^{-1}) and temperature (250 to 500 K) ranges in which testing was performed. The rate-limiting deformation mechanism in these ranges for these materials was predicted to be the formation and migration of kink pairs to move screw dislocations on the {112} slip systems.[1,5–11]

The modeling results show accurate predictions of the yield stresses of all five alloys (including two thicknesses

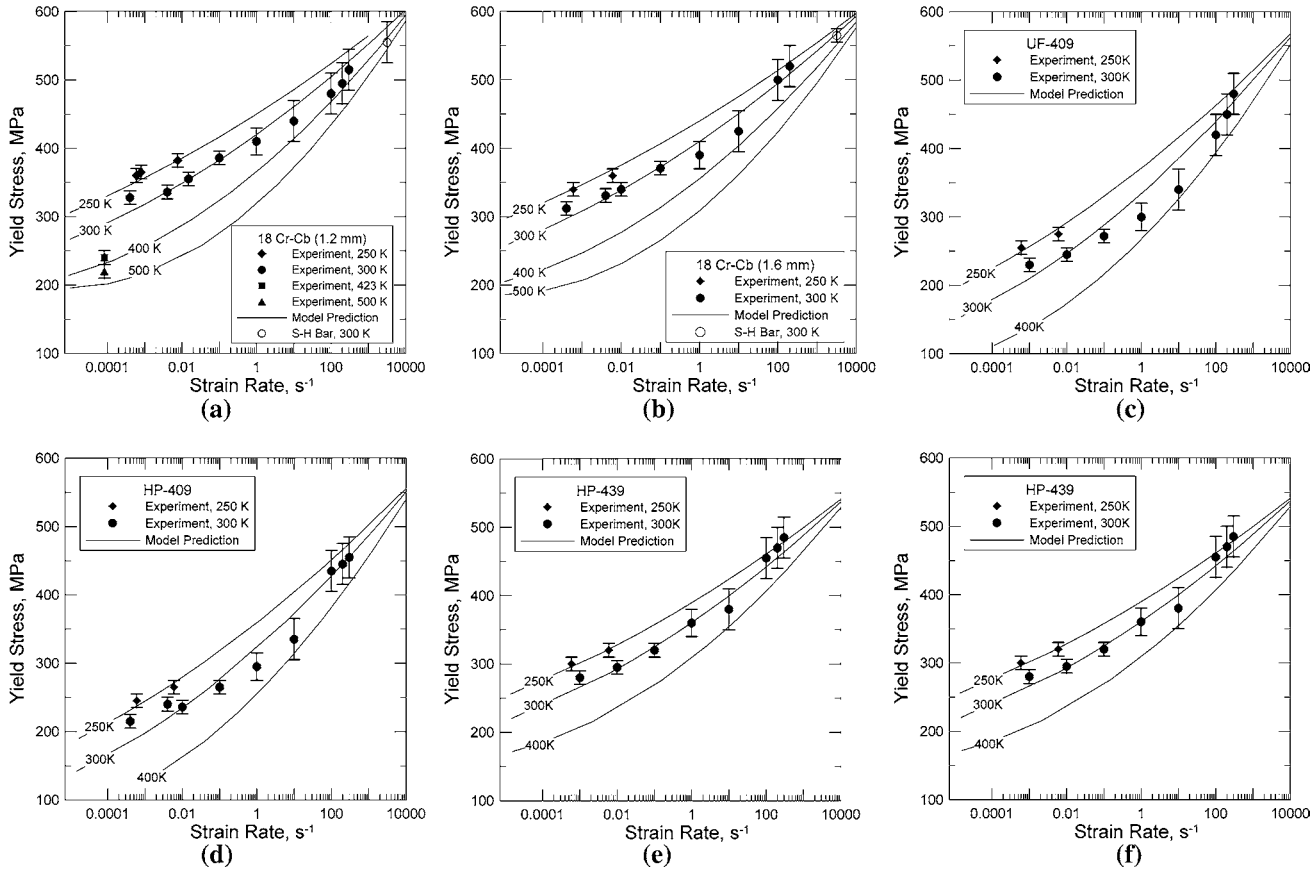

Fig. 5—Experimental 0.2 pct offset yield stress data plotted with controlled manual fit model predictions as a function of strain rate and temperature for (*a*) 18 Cr-Cb (1.2 mm), (*b*) 18 Cr-Cb (1.6 mm), (*c*) UF-409, (*d*) HP-409, (*e*) HP-439, and (*f*) Duracorr. The 18 Cr-Cb (1.6 mm) and (1.2 mm) points plotted at 3000 s^{-1} were determined from a Split–Hopkinson Bar compression test and were not used for the controlled manual model fit.

of 18 Cr-Cb) within the repeatability of the experimental tensile testing. These results support the applicability of the single deformation mechanism model for a wide range of substitutional alloy contents and strain rates. Also, the model results are in agreement with room-temperature experimental data for strain rates varying over six orders of magnitude, and for quasi-static tensile tests at 250, 423, and 500 K, although the nonambient tests were not used for the controlled manual curve fitting procedure. The model predicts continuously increasing strain rate sensitivity with increasing strain rate, as would be expected for a single deformation mechanism model.

Close agreement between the model and experimental results, in addition to the reasonable agreement of model parameters (Table II) with those reported in the literature and used to model pure ferritic iron suggest that the deformation mechanisms are the same for ferritic stainless steels as they are for mild steels at the strain rates and temperatures tested here. With regard to the model parameters, there is a large variation in the strain rate constant $\dot{\varepsilon}_o$ between the pure ferritic iron, niobium, and stainless steels. This is likely explained by the approximately two orders of magnitude range of dislocation densities that can occur in annealed metal[24] and the large variation in distance between insurmountable barriers (L) to dislocation movement that can occur with alloying. The dislocation density and distances between insurmountable barriers are both multiplied in the numerator (Eqs. [4] and [7]) in the determination of the strain rate constant.[6] It is therefore reasonable that this constant is lower for the stainless steels, as compared to pure ferritic iron, due to their higher alloying contents. The value of the strain rate constant for the niobium study[16] is significantly different from the values shown in the pure ferritic iron study[1] and in this study. The difference in the strain rate constant shows that this value can vary significantly with changes in Peierl's stress and distance.

The final modeling parameters suggest that for a given dislocation density and grain size, the alloy content is the primary factor that affects the yield stress when examining the bcc matrix ferritic stainless steels studied here. This suggestion is supported by Figures 6 and 7, which show that the effect of strain rate on each alloy is similar, *e.g.*, the flow stress at 0.1 strain and true stress at instability increase similarly in all materials as a function of strain rate. The lines shown in Figures 6 and 7 simply differentiate materials, and are not indicative of a curve fit. The curves in Figures 6 and 7 have a similar shape to the curves in regions II and IV in Figure 2. The true stresses at 0.1 strain and instability

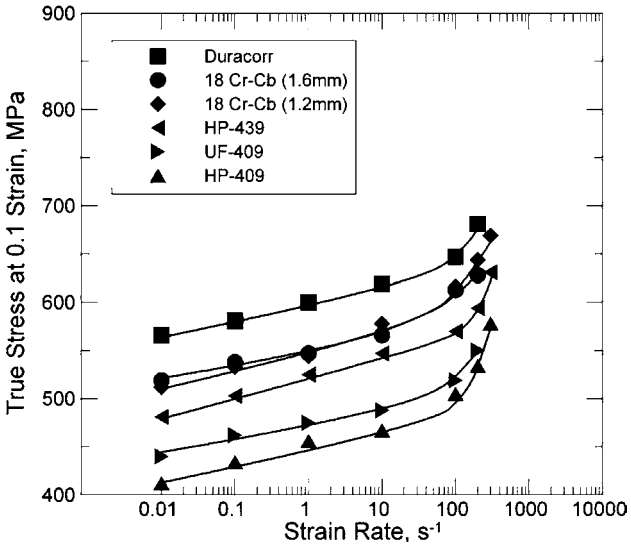

Fig. 6—Effect of strain rate on the true flow stress at 0.1 strain of all material conditions tested. Lines present differentiate materials and are not indicative of a curve fit.

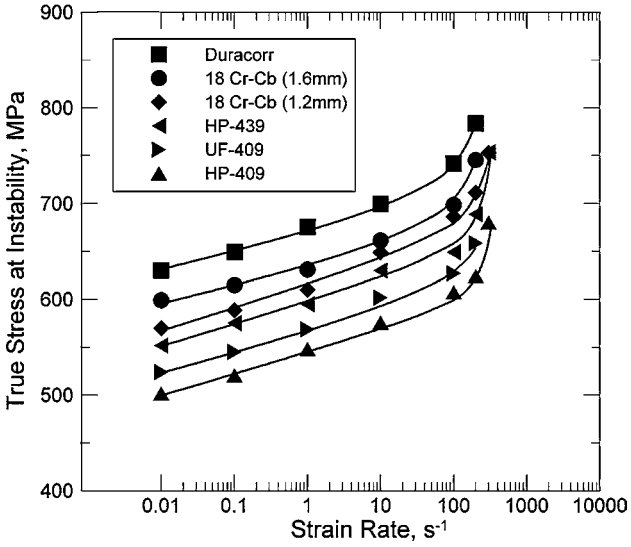

Fig. 7—Effect of strain rate on the true stress at instability for all material conditions tested. Lines present differentiate materials and are not indicative of a curve fit.

increase approximately linearly with the logarithm of strain rate to 100 s^{-1}.

At levels of strain above yield (such as 0.1 and instability) and at strain rates above approximately 1 s^{-1},[19,20] adiabatic conditions exist. The adiabatic temperature increase of the samples during testing was measured;[19,20] however, the data presented in Figures 6 and 7 have not been adjusted for temperature. It is acknowledged that the flow stress values at strain rates of 1 s^{-1} and higher in these plots will be slightly higher if corrected for adiabatic heating. The effect of adiabatic heating will increase slightly with strain rate.[19,20] It is therefore possible that, if corrected for adiabatic heating, the strain-rate-sensitivity curves in Figures 6 and 7 may have a discontinuity at a lower strain rate than is shown. This effect is likely to be relatively small, however, with maximum temperature increases on the order of 70 °C.[19,20] Nevertheless, it is clear in Figures 6 and 7 that there is a significant change in the slope of the flow stress *vs* strain rate curve above 100 s^{-1}, which may be indicative of a change in the mechanism of plastic flow in the samples at elevated strain rates. This may coincide with the change in active slip planes from {110} to {112} that is shown by Brunner and Diehl[1,5–10] as a function of temperature or strain rate.

C. *Alloying Effects*

In a dilute solid solution, the athermal shear stress is often considered to be independent of solute content;[12] however, in these steels, the solute content cannot be considered dilute. In nondilute solutions, it is theorized that the solute creates both long-range (athermal) and short-range (thermal) obstacles to dislocation motion, thus affecting the value of the athermal shear stress τ_G and the thermal shear stress τ^*.

It follows that the strengthening potency of the total solid solution alloy content of each material would correlate with the value of the athermal shear stress τ_G shown in Table II. Such a correlation requires an estimate of the relative solid solution strengthening potency of each alloying addition. The additive total solid solution strengthening contribution can be estimated by an approximation of relative alloy strengthening potency by assigning the strengthening potency of Cr arbitrarily as 1.0, and then basing the values of Ni, Mn, Si, Mo, and Nb on their relative strengthening power when compared to Cr. The relative multiplier values for Ni, Mn, and Si are taken from the literature[25] at room temperature, where Ni is 3 times as potent, and Mn and Si are 4 times as potent as Cr. Values of the multiplier for Mo and Nb were each estimated to be 4.[13] These values

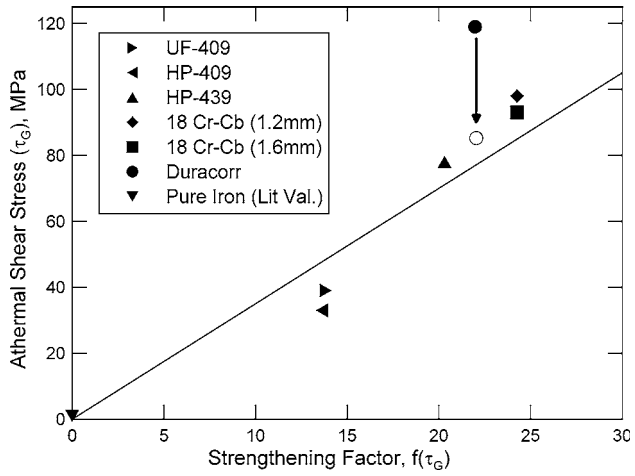

Fig. 8—Model parameter τ_G plotted *vs* a function of the relative strengthening capabilities of each substitutional alloying element. The strengthening factor $f(\tau_G)$ is based on composition of each alloy. The open symbol represents an *inferred* value of $f(\tau_G)$ for Duracorr based on a correction of the yield stress for grain size using the Hall–Petch relation.

Table III. Individual Contributions of Each Alloying Element on the Strengthening Factor $f(\tau_G)$

	Element Strengthening Factor Contribution (Weight Percent Multiplier)							
Alloy	Cr (1)	Ni (3)	Mn (4)	Si (4)	Mo (4)	Nb (4)	Total	Total Cr
HP-409	10.83	0.45	0.68	1.52	0.12	0.02	13.62	2.79
UF-409	11.18	0.42	0.72	1.36	0.12	0.02	13.82	2.64
HP-439	17.31	0.57	0.80	1.44	0.16	0.03	20.31	3.00
18 Cr-Cb	18.25	0.93	1.16	1.60	0.16	2.16	24.26	6.01
Duracorr	11.37	1.23	5.72	2.64	1.00	0.01	21.97	10.60

were then multiplied by the weight percent present in each alloy to determine a "strengthening factor" $f(\tau_G)$, which is plotted on the x-axis in Figure 8, and can be described by the following equation:

$$f(\tau_G) = 1\ \text{Cr (wt pct)} + 3\text{Ni} + 4\text{Mn} + 4\text{Si} + 4\text{Mo} + 4\text{Nb} \quad [13]$$

A summary of the individual contributions to the strengthening factor for each alloy is presented in Table III, which shows that the ferritic stainless steel alloys used for this study can be divided into three general alloy groups with respect to the strengthening factor $f(\tau_G)$. The group delineations are clear when the strengthening factor contribution of Cr is subtracted from the total strengthening factor, as shown in the last column of Table III. The alloy groups are as follows: (1) HP-409, UF-409, and HP-439 are primarily affected by Cr content, with relatively small contributions by Ni, Mn, Si, Mo, and Nb, where the non-Cr contribution is roughly constant; (2) 18 Cr-Cb has a higher Cr content with significantly higher contribution from Nb and slightly higher contributions from Ni, Mn, and Si, and the non-Cr contribution is approximately double that of the first group; and (3) Duracorr has a similar Cr to the first group, but significantly increased Ni, Mn, Si, and Mo, and the non-Cr contribution is nearly half of the total alloying contribution.

Figure 8 presents the model parameter τ_G plotted *vs* the strengthening factor (closed symbols) for each of the five ferritic stainless steel alloys and a literature value of τ_G for pure iron.[1] If the Duracorr alloy is not considered, the relationship between τ_G and the strengthening factor is approximately linear, indicating a direct relationship between the athermal shear stress and alloy content for two of the alloy groups described previously.

As discussed previously, Duracorr has a significantly smaller grain size than the other materials, which must be considered. The grain size effect for the Duracorr material is addressed with a calculation of the contribution of the grain size to the yield strength based on the Hall–Petch relationship (Eq. [12]).[18] For iron-based ferritic (bcc) alloys, values for k_y typically range between 5 and 25 MPa/mm$^{-1/2}$,[13,26,27] and it is reasonable to assume a value of 10 MPa/mm$^{-1/2}$ for these ferritic stainless steels. If the 0.01 s^{-1} 300 K yield stress for the Duracorr material is adjusted to a grain size of 20.0 μm (approximately the values of the other alloys) from 7.9 μm, the yield stress predicted by the Hall–Petch relation is 320 MPa. The adjusted yield stress for Duracorr is between the experimentally determined yield stresses of the HP-439 alloy (~290 MPa) and the 18 Cr-Cb alloys (~340 to 360 MPa). Because the value of τ_G for the materials with similar grain sizes varies directly with the yield strength, it follows that the value for τ_G for Duracorr with a similar grain size to the other alloys would fall between the values for HP-439 and 18 Cr-Cb, as shown with the open symbol in Figure 8. The adjusted τ_G (open symbol) has not been calculated, only *inferred* from the relative yield stresses. With the predicted correction for grain size and inferred τ_G value for Duracorr, Figure 8 shows a linear relationship between the strengthening factor and τ_G for all five alloys and all three alloy groups.

The correlation of τ_G to the strengthening factor is at best an estimate, but indicates that the values determined for τ_G based on experimental data and the model are consistent with those that may be ascribed due to solid solution strengthening. In this case, the materials are all ferritic stainless steels, and the solid solution contribution of the strengthening appears to be linear as a function of alloy content and a function of alloying element potency. In addition, this linear relationship exists for all three alloying groups (described previously), and that the results do not just apply to one type of alloying combination.

VI. CONCLUSIONS

From the tensile testing of five ferritic stainless steel alloys at strain rates ranging from 0.001 to 300 s^{-1} at room temperature and at quasi-static rates at 250, 423, and 500 K, and the application of a widely accepted model to the experimentally determined yield stress, the following important conclusions can be reached.

1. Similar strain-rate dependence was experimentally exhibited in the 0.2 pct offset yield stress, the true stress at 0.1 strain, and true stress at instability for all five ferritic stainless steel alloys in the strain rate and temperature regimes tested.
2. Experimentally determined yield stresses have been successfully fit to a fundamental deformation mechanism model for pure bcc materials, providing evidence that these ferritic stainless steels have the same deformation mechanism as pure ferritic iron and ferritic mild steels.
3. For the experimental data presented in this study, the model parameters H_k, α, $\dot{\varepsilon}_o$, and τ_G determined

for the ferritic stainless steels are found to be in reasonable agreement with respect to the values found previously for pure ferritic iron[1] and niobium.[16]
4. The deformation mechanism model previously developed by Seeger and Schiller[4] was applied to predict yield stress over a wide range of temperatures and strain rates, based on experimental results at one temperature (300 K). For the data presented in this article, the model accurately predicts with the experimental results (yield stresses) over the wide range of temperatures and strain rates. Therefore, it appears that this model should be useful as a constitutive relationship input for finite element analysis of production forming operations.
5. A correlation between alloying content and the athermal shear stress τ_G is made based on alloy strengthening contribution. This correlation suggests that mechanical property changes due to solid solution strengthening alloy additions can be successfully predicted with this model.

ACKNOWLEDGMENTS

The authors acknowledge the support of the Advanced Steel Processing and Products Research Center, an industry/university cooperative research center at the Colorado School of Mines. Special thanks are extended to AK Steel and Bethlehem Steel Company for supplying the materials used in this study. The authors also thank Dr. Carl Cady, Los Alamos National Laboratory, for performing Split–Hopkinson bar compression tests.

REFERENCES

1. D. Brunner and J. Diehl: *Phys. Status Solidi A*, 1991, vol. 124, pp. 155–70.
2. C.W. Kovach: *High-Performance Stainless Steels*, Nickel Institute, Toronto, ON, Canada, 2000, pp. 25–27.
3. *The Catalyst*, Armco Publication, Middletown, OH, 1997, Issue No. 3, p. 4.
4. A. Seeger and P. Schiller: in *Physical Acoustics*, W.P. Mason, ed., Academic Press, New York, NY, 1966, vol. IIIA, pp. 361–491.
5. D. Brunner and J. Diehl: *Strength of Materials*, ICSMA 10, Japan Institute of Metals, Sendai, Japan, Aug. 22–26, 1994, pp. 141–44.
6. D. Brunner and J. Diehl: *Phys. Status Solidi A*, 1987, vol. 104, pp. 145–55.
7. D. Brunner and J. Diehl: *Phys. Status Solidi A*, 1991, vol. 124, pp. 455–64.
8. D. Brunner and J. Diehl: *Phys. Status Solidi A*, 1991, vol. 125, pp. 203–16.
9. D. Brunner and J. Diehl: *Z. Metallkd.*, 1992, vol. 12 (83), pp. 828–34.
10. D. Brunner, J. Diehl, and A. Seeger: *Conf. Structure and Properties of Crystal Defects*, Liblice, Czechoslovakia, Elsevier Science Ltd., Oxford, UK, 1984, pp. 175–83.
11. W.A. Spitzig and A.S. Keh: *Metall. Trans.*, 1970, vol. 1, pp. 2751–57.
12. W.C. Leslie: *Metall. Trans.*, 1972, vol. 3, pp. 5–26.
13. W.C. Leslie: *The Physical Metallurgy of Steels*, Hemisphere Publishing, India, 1981, pp. 37–38, 118–19, 127, and 197.
14. T.Z. Blazynski: *Materials at High Strain Rates*, Elsevier Applied Science, New York, NY, 1987, pp. 133–48.
15. A. Seeger: *Conference Dislocations 1984 in Aussois, France, 8–17 March 1984*, Editions du Centre National de la Rechereche Scientifique, Paris, France, 1984.
16. F. Ackermann, H. Mughrabi, and A. Seeger: *Acta Metall.*, 1983, vol. 31 (9), pp. 1353–66.
17. A. Seeger: *Z. Metallkd.*, 1981, vol. 72, pp. 369–80.
18. G.E. Dieter: *Mechanical Metallurgy*, 3rd ed., McGraw-Hill, Inc, New York, NY, 1986, pp. 189–90.
19. K.D. Clarke: Master's Thesis, T-5635, Colorado School of Mines, Golden, CO, July, 2002.
20. K.D. Clarke, R.J. Comstock, Jr., M.C. Mataya, D.K. Matlock, J.G. Speer, and G.P. Martins: Technical Paper No. 2003-01-0526, Society of Automotive Engineers, Warrendale, PA, 2003.
21. D.M. Bruce: Ph.D. Thesis, T-5780, Colorado School of Mines, Golden, CO, July 2003.
22. D.M. Bruce, J.G. Speer, D.K. Matlock, and A. De: Technical Paper No. 2004-01-0507, Society of Automotive Engineers, Warrendale, PA, 2004.
23. I.D. Choi, D.M. Bruce, S.J. Kim, C.G. Lee, S.H. Park, D.K. Matlock, and J.G. Speer: *ISIJ Int.*, 2002, vol. 42 (12), pp. 1483–89.
24. R.E. Reed-Hill and R. Abbaschian: *Physical Metallurgy Principles*, 2nd ed., PWS Publishing Company, Boston, MA, 1973, p. 268.
25. W.C. Leslie, R.J. Sober, S.G. Babcock, and S.J. Green: *Trans. ASM*, 1969, vol. 62, pp. 690–710.
26. M.A. Meyers and K.K. Chawla: *Mechanical Behavior of Materials*, Prentice-Hall, Upper Saddle River, NJ, 1999, pp. 270–72.
27. T.H. Courtney: *Mechanical Behavior of Materials*, McGraw-Hill, New York, NY, 1990, pp. 169–73.